Polymer Vol. 37 No. 5, pp. 737–744, 1996

0032-3861/96/$15.00+0.00

Raman, infra-red and d.s.c. studies of lithium coordination in a thermoplastic polyurethane

A. Ferry* and P. Jacobsson
Department of Physics, Umeå University, S-901 87 Umeå, Sweden

and J. D. van Heumen and J. R. Stevens
Guelph–Waterloo Program for Graduate Work in Chemistry, University of Guelph, Guelph, Ontario, Canada N1G 2W1

Fourier transform (*FT*)-Raman and infra-red (i.r.) spectroscopy were utilized to monitor changes in the morphology of a commercial, phase-segregated thermoplastic polyurethane (TPU) as a function of $LiClO_4$ concentration (0.1 to 2.0 mmol/g TPU). Significant changes in both the *FT*-Raman and the *FT*i.r. spectra were detected which suggest a competition between hydrogen bonding and lithium cation coordination, especially between the hard segments of the host polymer matrix. A loss in long-range ordering of the hard domain was observed by differential scanning calorimetry with an increase in salt concentration. The ionic conductivity (σ) was found to increase with increasing temperature and salt concentration. For the highest concentration used, σ ranged from a very low value of $\sim 1 \times 10^{-9}\,S\,cm^{-1}$ at room temperature to $\sim 1 \times 10^{-4}\,S\,cm^{-1}$ at 130°C

(Keywords: polyurethane; *FT*i.r. spectroscopy; Fourier transform Raman)

INTRODUCTION

Pioneering work by Wright and co-workers[1] and Armand *et al.*[2] has inspired a large number of experimental investigations into the properties of polyether–alkali metal salt complexes. The main interest has been to enhance ionic conductivity; however, morphological studies have also been carried out since in many applications the polymer electrolyte is also required to exhibit elastomeric properties in addition to high ionic conductivity. Ionic transport occurs mainly through a coupling between the ions and polymer segmental motion[3], and early work, using poly(ethylene oxide) (PEO) as the host polymer, showed that ionic conduction takes place mainly in the amorphous regions of the polymer–salt complexes[4]. Therefore, to be useful, the polymer–salt electrolyte should be flexible (well above its glass transition temperature, T_g, in application), have a low degree of crystallinity and be thermodynamically and structurally stable. Such ambient temperature applications as solid-state batteries[5], fuel cells[6], smart windows and other electrochromic devices[7,8] are being considered.

Polymers and copolymers with a variety of polar groups (usually O, N, S) have been examined and it has been found that polymer electrolytes based on host polymer matrices incorporating oxyethylene chains (i.e. CH_2–CH_2–O repeat units) yield the highest ionic conductivities. Oxyethylene oligomers have been the most widely studied and were incorporated into macromolecules in a way that inhibits the crystallization of PEO[9,10]. Thermoplastic polyurethanes (TPUs) are diblock, flexible elastomers consisting of a soft phase (polyether or polyester) reinforced by condensation with a hard phase[11,12]. This phase-segregated morphology, in which the hard and soft phases are thermodynamically incompatible, promotes hydrogen bonding within the hard domain between urethane C=O and N–H moieties on adjacent polymer chain segments. However, complete phase segregation is never realized and, depending on the extent of phase intermixing, the boundary between the hard and soft domains is not well defined. Consequently the elastomeric properties of the TPU vary with a number of variables, including soft segment molecular weight and hard segment concentration[12].

Although TPUs have been used previously as matrices for ionic conduction, it is unclear how the phase-segregated morphology of the TPU is affected by incorporation of ionic salts. Numerous studies have attempted to elucidate the relationships between structure and properties within thermoplastic polyurethanes, principally by use of nuclear magnetic resonance spectroscopy[13,14], small-angle X-ray scattering[15–17], differential scanning calorimetry (d.s.c.)[18–21] and Fourier transform infra-red (*FT*i.r.) spectroscopy[22–26]. D.s.c. measurements have previously shown that polyurethanes of hard segment concentration greater than 40% exhibit three endothermic transitions, above the additional low

* To whom correspondence should be addressed

temperature T_g of the soft segment[19]. Assignments for these transitions are generally accepted as involving short-range ordering in the hard domain (t_1), long-range ordering (t_2) and microcrystallinity in the hard domain in the TPUs of high hard segment concentration (t_3)[21]. Seki and Sato[27] and McLennaghan and co-workers[28,29] have shown that ionic salt doping of TPUs results not only in the expected increase in the soft segment T_g, but also in a loss of the higher temperature endothermic transitions.

Several investigations have examined the hydrogen bonding characteristics of phase-segregated polyurethanes by *FT*i.r.[22–26]. The main regions of interest are the N–H region, with characteristic bands at ~ 3320 and $3420\,cm^{-1}$ corresponding to hydrogen-bonded and free N–H groups, and the carbonyl region which is defined by three carbonyl stretching vibrations: the non hydrogen-bonded C=O ($1732\,cm^{-1}$) and two stretching vibrations associated with disordered ($1712\,cm^{-1}$) and ordered ($1700\,cm^{-1}$) hydrogen-bonded C=O[25,26].

In this work, Fourier transform near infra-red Raman spectroscopy (*FT*-Raman) is utilized as a complement to *FT*i.r. along with d.s.c. and impedance spectroscopy (IS) measurements to study the effects of salt concentration and temperature on the phase morphology and bulk impedance of a TPU of composition MDI/BDO/PTMO [methylene bis(phenyl-isocyanate)/1,4-butanediol/poly-(tetramethylene oxide)] doped with $LiClO_4$. Two-dimensional covariance analysis of spectral variations is used to highlight interactions between the dissolved salt and the polymer host matrix.

EXPERIMENTAL

The TPU examined in this investigation (Estane 5714, B.F. Goodrich Co.) contains a PTMO soft segment and a hard segment of MDI and BDO, and was used as received. The solvents, dimethyl formamide (DMF) (Fischer) and tetrahydrofuran (THF) (Fisher), were dried over 4 Å molecular sieves. The dopant salt, $LiClO_4$ (Aldrich), was dried under reduced pressure (10^{-3} torr) for 24 h at 110°C.

Solutions of various salt concentrations were prepared by dissolving both salt and TPU in DMF at 10 mass%. The solution was cast on to Teflon plates and the solvent was then slowly removed under reduced pressure for a minimum of 24 h at 120°C. For *FT*i.r. analysis, solutions containing 5 mass% of polymer and salt in THF were prepared. The solution was cast directly on NaCl plates and the solvent was evaporated via a slow reduction of pressure at 110°C for 24 h. Prior to *FT*-Raman measurements the samples were again carefully dried for a minimum of 24 h at 120°C under reduced pressure ($\sim 10^{-3}$ torr) to ensure that no absorbed water was present.

D.s.c. measurements were made over the temperature range −100 to 200°C using a Du Pont 2910 DSC instrument at a heating rate of $10°C\,min^{-1}$. The annealing experiments were conducted in the calorimeter at 140°C for 45 min prior to commencing the temperature sweep.

Impedance measurements were performed using thin films prepared by solvent evaporation with a diameter of 17 mm and an approximate thickness of 0.15 mm. Actual thickness measurements were conducted in the impedance cell by a micrometer device mounted as part of the cell construction. The ionic conductivities of the TPU, sandwiched between two stainless steel electrodes, were measured using a Hewlett–Packard 4192A impedance analyser interfaced with an HP series 300 computer for remote data collection.

FT-Raman spectra with a wavenumber resolution of $2\,cm^{-1}$ were recorded at 25°C with the temperature stability in the sample estimated to be ±0.3°C. The spectra were recorded in a Bruker IFS 66 with a Raman module FRA 106 and a continuous Nd:YAG laser (1064 nm) using a 180° backscattering geometry. During measurements, the sample cell was placed in an evacuated thermostat. To compensate for differences in overall signal intensity due to varying sample thickness and sample composition, all *FT*-Raman spectra were normalized to the integrated area of the symmetric stretch C=C aromatic breathing mode at $\sim 1616\,cm^{-1}$ which was not affected by the introduction of lithium salt into the polymer matrix. Curve fits to the spectra were obtained by analysis with Peakfit software (Jandel Inc.).

*FT*i.r. spectra were recorded at ambient and elevated temperatures using a Nicolet system 4.4 instrument with a wavenumber resolution of $2\,cm^{-1}$. Curve fits to the resulting spectra were obtained by analysis with Grams 386 software (Galactic Industries Corp.) with a maximum error associated with the fit estimated to be ±15%. Where bands are well resolved the approximate error in calculating the band intensity is less than 10%.

Covariance analysis

As suggested by Noda and co-workers[30], correlated spectral changes in highly overlapped band envelopes, induced by some external perturbation, can be resolved by spreading out the information over a second spectral dimension in a so-called two-dimensional (2D) covariance map. A 2D covariance map is generated in the following manner from a set of n spectra, $A_j(\nu)$, where $j = 1, \ldots, n$. The set of spectral data is first mean centred by subtracting the average of all the spectra in the set from each individual spectrum. Thus, the mean centred set of spectra, $\tilde{A}_j(\nu)$, is given by

$$\tilde{A}_j(\nu) = A_j(\nu) - A_{\text{mean}}(\nu) \tag{1}$$

The 2D covariance spectrum, $C(\nu_1, \nu_2)$, is defined as

$$C(\nu_1, \nu_2) = \frac{\sum_{j=1}^{n} \tilde{A}_j(\nu_1)\tilde{A}_j(\nu_2)}{n-1} \tag{2}$$

The 2D covariance map is then simply a contour plot of $C(\nu_1, \nu_2)$ for all pairs of wavenumbers ν_1 and ν_2 in which correlated spectral variations will appear as regions of positive or negative covariance. The extension of the 2D covariance analysis to incorporate correlated spectral responses acquired from different spectroscopic techniques is straightforward, as long as the perturbation applied to the sample is the same[31].

In this work, *FT*i.r. and *FT*-Raman spectra corresponding to different salt concentrations were correlated using MATLAB software (The MathWorks, Inc.), in order to highlight spectral variations induced by the introduction of ionic salt into the polymer host matrix. The resulting covariance spectra are presented as 2D contour maps of positive and negative covariance.

Table 1 D.s.c. data for the TPU–$LiClO_4$ complexes

$LiClO_4$ mmol/g TPU	T_g (°C)[a]	$\Delta T_g/\Delta c$ (°C/mmol/g TPU)	t_1 (°C)	t_2 (°C)	t_4[b] (°C)	ΔH_m (J/g)
0.0	−44	–	108	150	156	2.6
0.30	−35	30	66	131	158	0.18
0.67	−22	90				
1.2	−19	20				
2.0	−12	10				

[a] When blanks occur in the table, no transitions were observed
[b] Only observed after annealing at 140°C for 45 min

RESULTS

D.s.c.

D.s.c. was utilized to examine the effect of $LiClO_4$ on the morphologically based thermal transitions of the TPU as well as on the polyether soft segment T_g. The results are presented in *Table 1*, which indicates an increase in the T_g of the PTMO soft segments as a function of salt concentration. This is consistent with other investigations of $LiClO_4$ doped TPUs containing either PEO[28,29] or poly(propylene oxide)[32,33] as the soft segment. By normalizing the T_g data with respect to concentration we obtain $\Delta T_g/\Delta c$ (*Table 1*) at each measurement. It is found that T_g does not increase linearly with increase in salt concentration; $\Delta T_g/\Delta c$ generally decreases and T_g is tending towards a plateau. This could be accounted for by the availability of ether oxygens and the plasticizing effect of increased ion association as the salt concentration is increased[33,34]. The results of Stevens and Schantz[35] show the plateau at high concentrations for T_g plotted as a function of salt concentration. The main plasticizers are charge neutral contact ion pairs which do not form transient crosslinks.

Table 1 also shows that after annealing the TPU at 140°C for 45 min, t_1 and t_2 coalesce into a single transition t_4 (~ 157°C). This new transition corresponds to the enhancement of long-range order; however, the endotherm is no longer observed for salt concentrations above 0.3 mmol/g TPU, indicating a loss of long-range order upon complexation with the lithium salt.

Impedance spectroscopy

Figure 1 illustrates the concentration dependency of the ionic conductivity, σ, for the TPU/$LiClO_4$ system and it is seen that the ionic conductivity increases with increase in temperature and increase in salt concentration over the concentration range investigated. At room temperature $\sigma \approx 10^{-9}\,S\,cm^{-1}$. The temperature dependency of the conductivity data is usually analysed during the Vogel–Tammann–Fulcher (VTF) or Arrhenius phenomenological relationships:

$$\sigma(T) = AT^{-1/2}\exp[-B/k_B(T - T_0)] \quad \text{(VTF)} \quad (3)$$

$$\sigma(T) = A\exp[-E/k_BT] \quad \text{(Arrhenius)} \quad (4)$$

In equations (3) and (4) A is constant, B is the pseudo-activation energy related to polymer segmental motion, T_0 is a reference temperature usually associated with the ideal glass transition temperature at which free volume disappears, and E is the activation energy for ionic hopping when the ionic motion is decoupled from the polymer host. Generally speaking, the VTF relation holds at higher temperatures and is a signature of the coupling between ions and polymer segmental motion; this is the basis for ionic conduction. At temperatures approaching T_g thermally activated hopping becomes

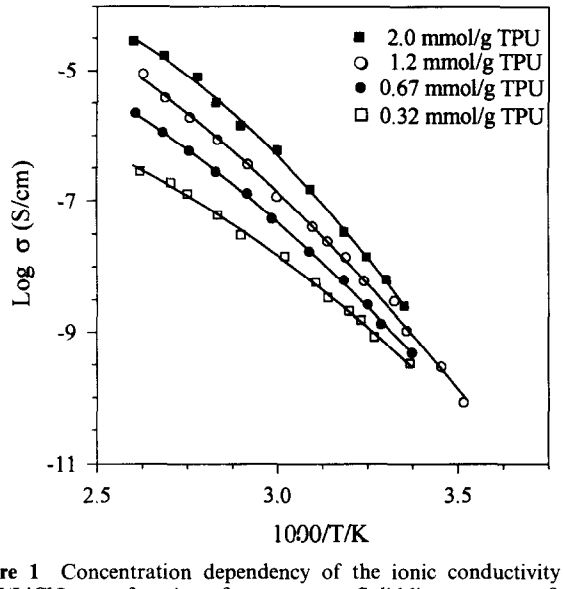

Figure 1 Concentration dependency of the ionic conductivity for TPU/$LiClO_4$ as a function of temperature. Solid lines represent fits to the conductivity data using the VTF equation

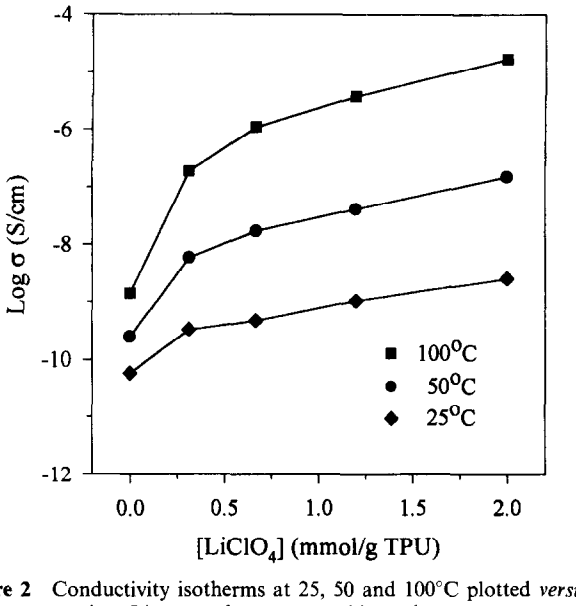

Figure 2 Conductivity isotherms at 25, 50 and 100°C plotted *versus* salt concentration. Lines are drawn as a guide to the eye

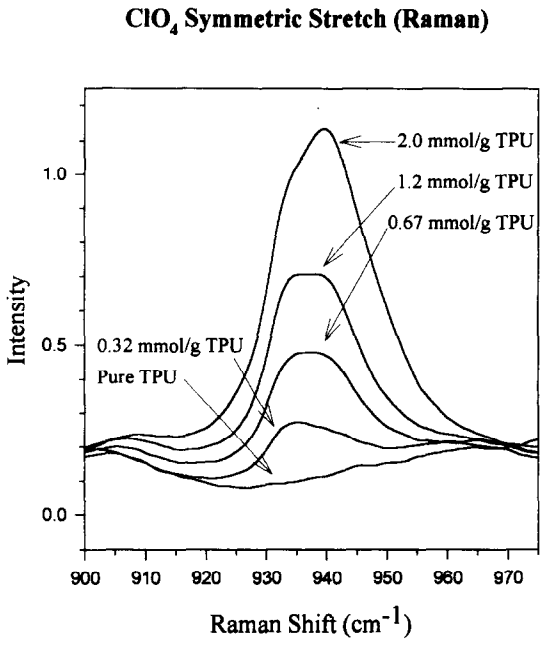

Figure 3 Raman spectra of the region containing the symmetric stretch of the perchlorate anion

dominant as the ions decouple from the polymer segmental motion, the average relaxation rate of which is now becoming slower than the ion hopping rate[36]. Plots of log σ *versus* reciprocal temperature are closest to VTF behaviour in the temperature range used, as illustrated in *Figure 1*. The log σ values for the 1.2 mmol/g TPU are slightly more linear with reciprocal temperature. *Figure 2* shows conductivity isotherms for the TPU/$LiClO_4$ system. Unlike in other studies of TPU/$LiClO_4$ systems[27,29,33] and TPU/$LiCF_3SO_3$[29,37], no maximum in σ is observed at a particular critical concentration. Preliminary experiments indicate that this maximum occurs at higher concentrations.

FT-*Raman spectroscopy*

Three spectral regions have been investigated: (1) 975 to 875 cm^{-1} containing the symmetric stretching mode of the perchlorate anion; (2) the ether oxygen region between 1200 to 1000 cm^{-1} which contains the C–O–C stretch for the PTMO phase ($\sim$ 1115 cm^{-1}) and the C(O)–O–C stretch of the hard phase ($\sim$ 1080 cm^{-1}); and (3) 1800 to 1650 cm^{-1} containing the C=O symmetric stretch vibration (amide I band).

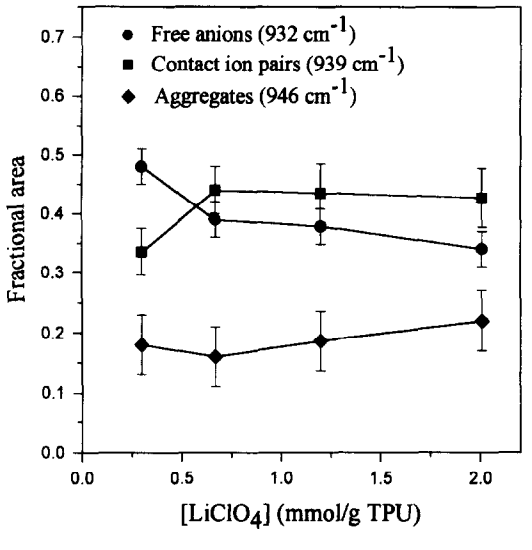

Figure 4 Relative amounts of different ionic species present as determined from curve fits to Raman spectra of the symmetric perchlorate anion band. Lines are drawn as a guide to the eye

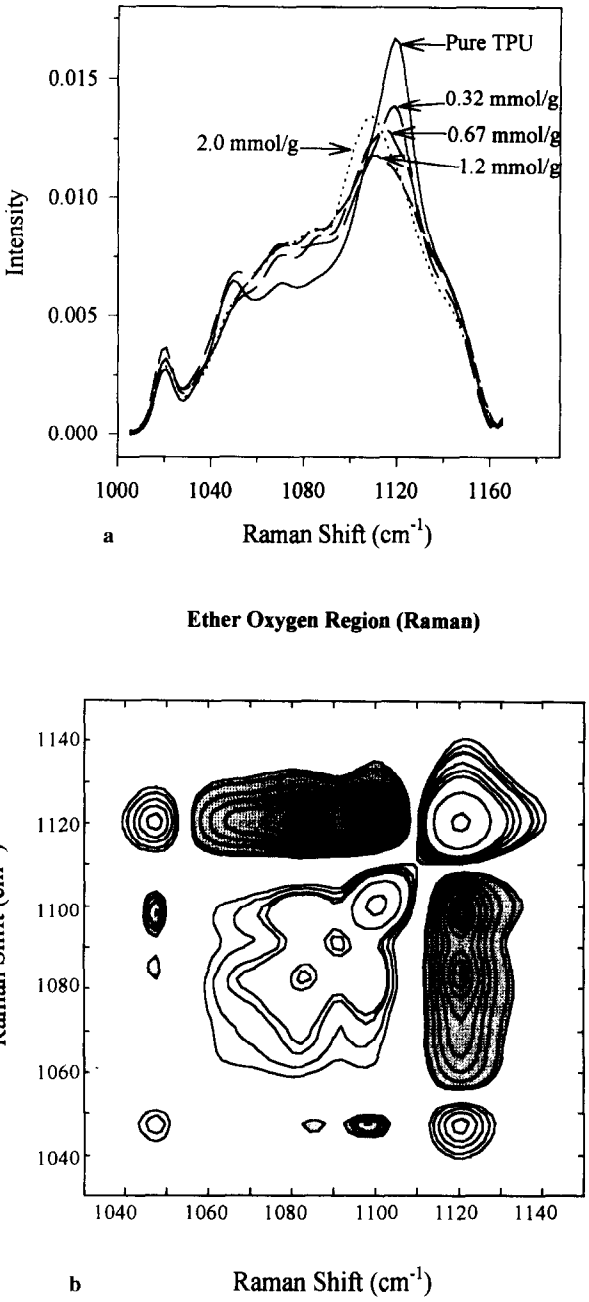

Figure 5 (a) Normalized Raman spectra of the ether oxygen region corresponding to different salt concentrations. The spectra have been correlated for a linear background term. (b) Calculated covariance spectrum (Raman *versus* Raman) of the ether oxygen region upon complexation with $LiClO_4$ represented as a contour plot. Regions corresponding to positive correlations are open, negative correlations are shaded

975 cm^{-1} to 875 cm^{-1}. The strong Raman band at $\sim$ 930–940 cm^{-1} corresponds to the symmetric stretch of the ClO_4 anion. As seen in *Figure 3*, the band is split, indicating different ionic environments for the perchlorate anions. According to previous assignments[38], the

low frequency band at $\sim 932\,cm^{-1}$ corresponds to free anions, the component at $\sim 939\,cm^{-1}$ corresponds to contact ion pairs and the broad high frequency component at $\sim 943\,cm^{-1}$ corresponds to higher order aggregates. In *Figure 4* the concentration dependency of the relative amounts of anionic species present is illustrated, as determined from a three-component analysis of the band envelopes after subtraction of the polymer background. It is seen that the fraction of 'free' anions decreases with increasing concentration.

1200 cm^{-1} to 1000 cm^{-1}. The ether oxygen region is clearly affected by the introduction of $LiClO_4$ into the polymer matrix, see *Figure 5a*. However, in the 1000 to $1165\,cm^{-1}$ region there are several overlapped bands and curve fits to the spectra necessarily comprise large uncertainties. To monitor changes with increasing salt concentration, the spectral variations were correlated. As seen in a contour plot of the correlation spectrum, *Figure 5b*, there are five Raman bands that are affected by the introduction of lithium salt into the polymer matrix. These bands are located at $\sim$ 1050, 1085, 1093, 1105 and $1120\,cm^{-1}$. According to the literature[22],the i.r. band corresponding to the C–O–C stretch of the PTMO phase is observed at $\sim 1115\,cm^{-1}$ and the C(O)–O–C stretch of the hard segment moiety at $\sim 1080\,cm^{-1}$ in the undoped TPU. From *Figure 5a* and *b* it is seen that the shaded feature at $\sim 1120\,cm^{-1}$ decreases in intensity with increasing salt concentration; this decrease is coupled to a relatively smaller increase of the band at $\sim 1080\,cm^{-1}$ with a levelling off. The feature at $\sim 1105\,cm^{-1}$ which increases with increasing salt concentration is likely to be the $\nu_3(F_2)$ band of the perchlorate anion[39].

1800 cm^{-1} to 1570 cm^{-1}. This region contains the carbonyl symmetric stretch vibration which consists of three characteristic bands assigned in pure TPUs as follows: (1) at $\sim 1700\,cm^{-1}$ corresponding to the ordered hydrogen-bonded species in the hard phase; (2) at $\sim 1713\,cm^{-1}$ corresponding to the disordered hydrogen-bonded species; and (3) at $\sim 1730\,cm^{-1}$ corresponding to 'free' carbonyl groups[25,26]. The region also includes the aromatic breathing mode symmetric stretch vibration (C=C) at $\sim 1616\,cm^{-1}$ which was used to normalize the *FT*-Raman spectra.

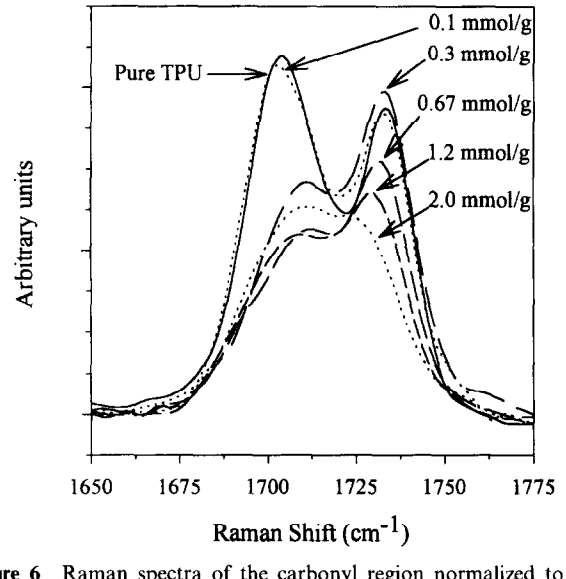

Figure 6 Raman spectra of the carbonyl region normalized to the aromatic breathing mode at $1616\,cm^{-1}$

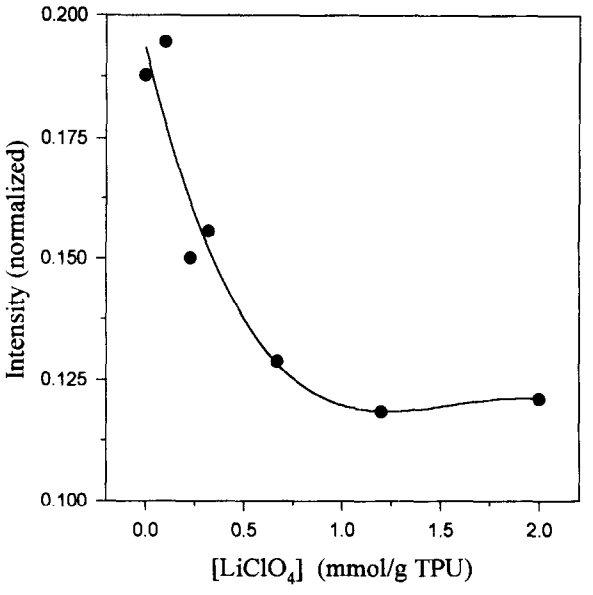

Figure 7 Total normalized area of the carbonyl region as a function of salt concentration (Raman). The line is drawn as a guide to the eye

The three characteristic modes of the carbonyl region are clearly affected by complexation with the lithium salt, see *Figure 6*. The total normalized integrated area of the C=O region is plotted against concentration in *Figure 7*. It is seen that the total intensity drops sharply with increasing salt concentration up to 0.67 mmol/g TPU, whereafter it levels off. This indicates that there is some interaction between the hydrogen-bonded carbonyl groups and the lithium salt which changes the scattering cross-section of this moiety. The band corresponding to the free carbonyl stretch at $\sim 1732\,cm^{-1}$ is readily

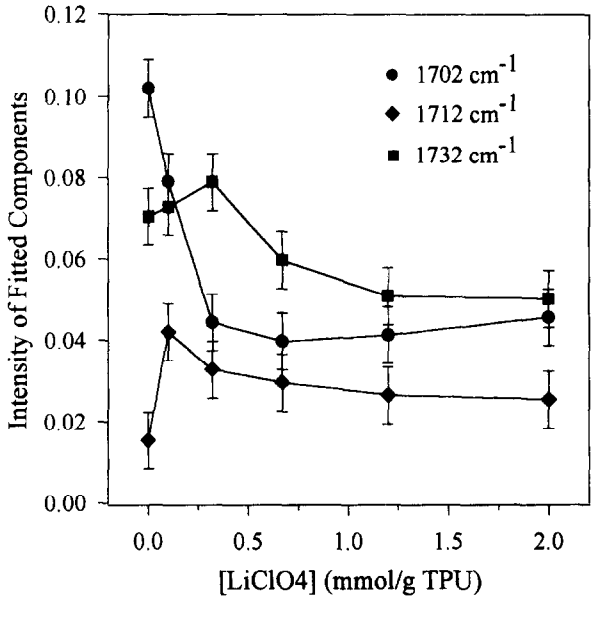

Figure 8 Concentration dependency of the integrated intensities of the three components in the normalized Raman spectra of the carbonyl region as determined from curve fits. Lines are drawn as a guide to the eye

resolved and in *Figure 8* it is seen that the intensity of this band first increases and then decreases slightly with increasing salt concentration. The band at $1702\,cm^{-1}$ drops by ~50% in intensity with the initial addition of salt to the system and then levels off at higher concentrations. The band at $1712\,cm^{-1}$ doubles in intensity with the initial addition of salt and then falls off slightly.

FT*i.r. spectroscopy*

Three i.r. regions have been examined: (1) 3600 to $3100\,cm^{-1}$ containing the hydrogen-bonded N–H stretching mode and the 'free' N–H stretch; (2) 1750 to $1650\,cm^{-1}$ containing the carbonyl symmetric stretch vibration or amide I band; and (3) 1150 to $1000\,cm^{-1}$ which contains the C–O–C stretch ($1115\,cm^{-1}$) and for the PTMO phase and the C(O)–O–C stretch ($1080\,cm^{-1}$) of the hard phase. The i.r. spectra were normalized to the CH_2 region (3000 to $2770\,cm^{-1}$) in order to compensate for differences in signal intensity due to varying sample thickness and sample composition.

$3600\,cm^{-1}$ to $3100\,cm^{-1}$. The N–H region is defined by at least two modes in an undoped TPU. The first at $3400\,cm^{-1}$ is assigned to the free N–H stretching vibration while the second is assigned to the hydrogen-bonded N–H stretch at $3310\,cm^{-1}$ (ref. 25). In the present investigation, the N–H region was affected by complexation with the lithium salt; however, curve fits to the highly overlapped features were difficult to obtain with any accuracy. According to the literature, the absorptivity

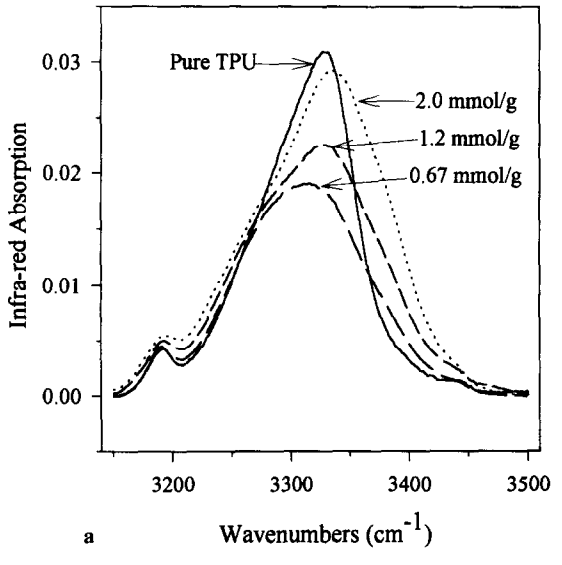

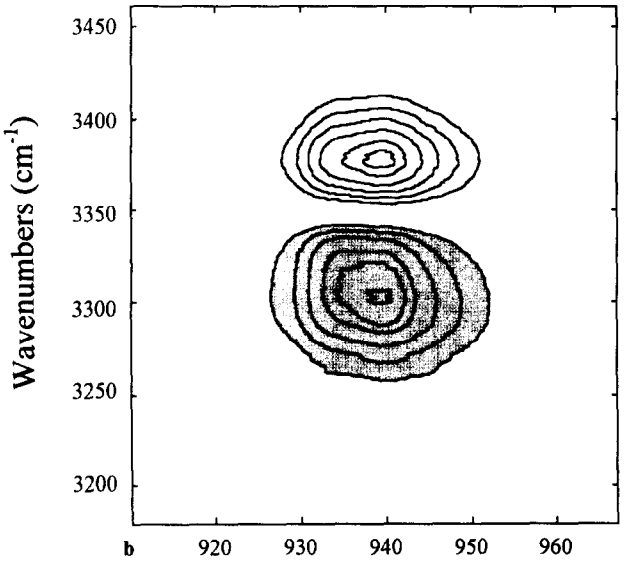

Figure 9 (a) I.r. spectra of the N–H region corresponding to different salt concentrations. The spectra have been corrected for a linear background term. (b) Covariance spectrum of the correlation between the N–H region (i.r.) and the perchlorate anion symmetric stretch at ~ $930\,cm^{-1}$ (Raman) for different salt concentrations represented as a contour map. Regions corresponding to positive correlations are open, negative correlations are shaded

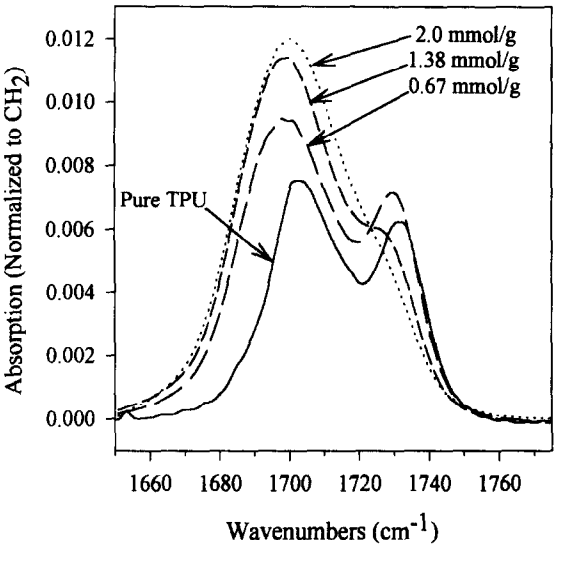

Figure 10 The carbonyl region (i.r.)

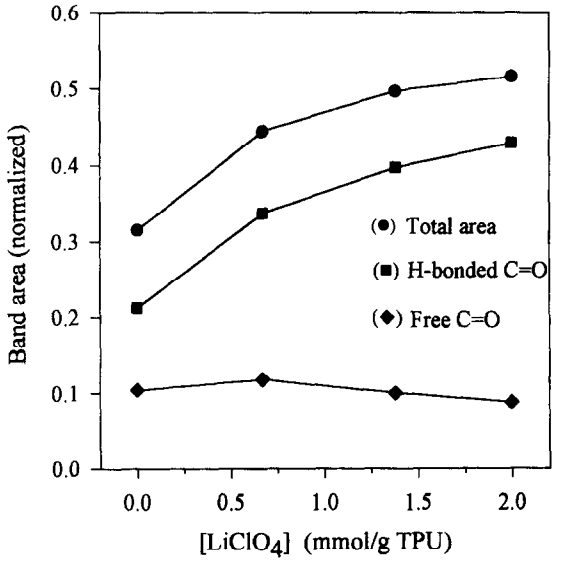

Figure 11 Concentration dependencies of the bands in the carbonyl region (i.r.): integrated intensity of the free C=O band ($1732\,cm^{-1}$), the sum of the intensities for the hydrogen bonded species (1712 and $1700\,cm^{-1}$) and the total carbonyl band area. Lines are drawn as a guide to the eye

coefficient for the hydrogen-bonded N–H band is a strong function of hydrogen bond strength[25,26] and therefore quantitative estimates of functional group concentration from band areas in the N–H region may be erroneous. For all concentrations, a weak band at $\sim 3440\,cm^{-1}$ corresponding to the free N–H band is observed. Significant changes are found in the region in between 3400 and $3250\,cm^{-1}$ which includes the hydrogen-bonded stretch at $3310\,cm^{-1}$, see *Figure 9a*. To illustrate the observed changes, the 3100 to $3500\,cm^{-1}$ region was normalized to unit area for all salt concentrations and the resulting spectra were correlated to the salt peak at ~ 930–$940\,cm^{-1}$ in the corresponding Raman spectra. The result is shown in *Figure 9b*. In the unshaded new feature at $\sim 3375\,cm^{-1}$ the intensity increases with increasing salt concentration whereas for the shaded feature at $\sim 3310\,cm^{-1}$, corresponding to the hydrogen-bonded N–H, the intensity decreases upon complexation with the lithium salt.

1750 cm^{-1} to 1650 cm^{-1}. *Figure 10* illustrates the effect of increase in salt concentration on the three characteristic i.r. modes of the carbonyl region. It is seen that the free carbonyl ($1730\,cm^{-1}$) band first increases slightly and then decreases with increasing salt concentration, whereas the two bands corresponding to hydrogen-bonded carbonyl groups in the ordered and disordered phases (1700 and $1712\,cm^{-1}$) increase in intensity. However, these two bands are difficult to resolve and in *Figure 11* the sum of these two components is plotted against concentration rather than the individual components. As seen in *Figure 11*, the total normalized integrated area of the C=O region increases sharply with increasing salt concentration, contrary to the observed decrease in the corresponding Raman spectra.

1200 cm^{-1} to 1000 cm^{-1}. Bands are observed at $1112\,cm^{-1}$ (C–O–C stretch) and $\sim 1080\,cm^{-1}$ (C(O)–O–C stretch). The relative area of the $1112\,cm^{-1}$ band decreases and the relative area of the C(O)–O–C band increases with increasing salt concentration. The feature at $1082\,cm^{-1}$ in the undoped TPU shifts to $1070\,cm^{-1}$ at the highest salt concentrations. This behaviour is consistent with an earlier study[40] on $LiCF_3SO_3$/TPU.

DISCUSSION

Dissolution of $LiClO_4$

The fraction of 'free' ions decreases and the fraction of contact ion pairs and ion aggregates increases with concentration in a more pronounced manner than for poly(propylene glycol) ($MW = 4000$)/$LiClO_4$ (ref. 41). This is probably due to the presence of hydroxyl groups in the latter system[42].

Lithium cation coordination to polar hard domains of the TPU

From a comparison with the Raman spectrum of pure $LiClO_4$ salt, it is clear that the salt has been solvated since no peaks associated with the crystal structure are observed in the spectra of the TPU/$LiClO_4$ complexes. *Figure 4* illustrates that there are free perchlorate anions present in the system even at the highest salt concentration investigated. *Figures 5* to *11* clearly show that the addition of $LiClO_4$ affects the N–H, C=O and C–O–C regions. Preliminary conclusions indicate that there is a preferred lithium cation coordination to the hard segment (N–H and C=O moieties) for $LiClO_4$ and to the soft segment C–O–C for $LiCF_3SO_3$/TPU[40].

The fact that the carbonyl region is affected by the introduction of $LiClO_4$ in both the Raman and the i.r. data suggests a coordination between the carbonyl oxygen and the Li^+ cation. The behaviour of the bands at ~ 1700 and $\sim 1712\,cm^{-1}$ with increasing salt concentration and the behaviour of the total integrated band area of the carbonyl region differs between the two methods (compare *Figures 6*, *7* and *8* with *Figures 10* and *11*). A similar effect has previously been observed for $LiClO_4$ dissolved in DMF, where a dramatic decrease in the carbonyl intensity with salt addition was observed in Raman but not in i.r.[43]. Differences between the Raman and i.r. spectra probably arise from the fact that Raman scattering is related to the rate of change of the polarizability tensor with the normal coordinates as the molecule vibrates whereas the i.r. absorption is related to the rate of change of the dipole moment. Thus Raman measurements give $\langle P_2(\hat{u}(0), \hat{u}(t))\rangle$ and i.r. absorption measurements give $\langle P_1(\hat{u}(0)\cdot\hat{u}(t))\rangle$ where P_1 and P_2 are first- and second-order Legendre polynomials and $\hat{u}$ is the unit vector along the molecular transition dipole[44]. It is unclear as yet how the Li^+ cation alters the electronic charge distribution, especially in the carbonyl region, to affect the polarizabilities and dipole moments differently. Further experimental work is proceeding to elucidate the concentration dependency of the total carbonyl band intensity.

The trend observed in *Figure 8*, in which the disordered and ordered hydrogen-bonded carbonyls are immediately affected by the addition of $LiClO_4$, with the intensity from the ordered region decreasing and that from the disordered phase increasing with increased concentration, is consistent with the disappearance of long-range ordering as observed in d.s.c. (*Table 1*).

It is interesting to note that neither the 'free' N–H stretch nor the free carbonyl stretch is affected to any greater extent by the introduction of lithium salt into the polymer matrix, but only bands assigned to hydrogen-bonded species. Thus we conclude that Li^+ cation coordination competes with hydrogen bonding. The new feature at $\sim 3375\,cm^{-1}$ has been observed previously[40] and is believed to be related to the coordination of the lithium cation with the urethane electron-rich nitrogen.

The Raman results in the ether oxygen region agree with the findings of van Heumen and Stevens[40] for a similar system where the TPU was doped with $LiCF_3SO_3$. In *Figures 5a* and *b* Raman spectra of the ether oxygen region corresponding to different salt concentrations are shown along with a 2D contour map of the calculated covariance spectrum. It is seen that the feature at $\sim 1120\,cm^{-1}$, corresponding to the soft PTMO segments, decreases with increasing salt concentration while the features at ~ 1085 and $1105\,cm^{-1}$ increase in intensity. In the i.r. spectra of the ether oxygen region the C(O)–O–C symmetric stretch frequency decreases from 1082 to $1070\,cm^{-1}$, indicating an inductive withdrawal of electron density from the ether linkage through the C=O by the Li^+ cation. This may well reflect the coordination of the lithium cations to both the C–O–C and the C=O moieties.

CONCLUSIONS

The addition of $LiClO_4$ to a commercial Estane TPU produces significant changes in both the Raman and the i.r. spectra. The changes are associated with those regions in the hard segments (N–H, C=O) where there is hydrogen bonding and the expected changes in the soft segment due to the well-known coordination of Li^+ to the ether oxygens. Since there is less change in the intensities of the free N–H and C=O symmetric stretch vibrations, we conclude that Li^+ coordination competes with hydrogen bonding and that the TPU becomes less ordered in the hard domain region and thus less elastomeric with increase in salt concentration. A reduced long-range ordering will also increase the flexibility of individual chain segments. This may influence the ionic conductivity, which was found to increase in temperature and salt concentration over the entire salt concentration range investigated. (The highest concentration, 2.0 mmol/g TPU, is equivalent to an ether oxygen to alkali metal cation ratio of < 8:1.) Experiments are in progress to study the temperature variation of the Raman and i.r. spectra in an attempt to understand the observed differences in the carbonyl region.

ACKNOWLEDGEMENTS

This work has been supported by grants from J C Kempes minnes stipendiefond and B. F. Goodrich, which are hereby gratefully acknowledged. J. D. van Heumen acknowledges support from the Ontario Centre for Materials Research.

REFERENCES

1 Fenton, D. E., Parker, D. E. and Wright, P. V. *Polymer* 1973, **14,** 589
2 Armand, M. B., Chabagno, J. M. and Duclot, M. J. in 'Fast Ion Transport in Solids' (Eds P. Vashista, J. N. Mundy and G. K. Shenoy) Elsevier North Holland, New York, 1979, p. 131
3 Ratner, M. A. and Shriver, D. F. *Chem. Rev.* 1988, **88,** 109
4 Harris, C. S., Shriver, D. S. and Ratner, M. A. *Macromolecules* 1986, **19,** 987
5 Gauthier, M., Belanger, A., Kapper, B., Vassort, G. and Armand, M. in 'Polymer Electrolytes Review 2' (Eds J. R. MacCallum, C. A. Vincent), Elsevier, London, 1989, p. 285.
6 Anderson, A. M., Stevens, J. R. and Granqvist, C. G. in 'Large Area Chromogenics—Materials and Devices for Transmittance Control Vol. IS4 (Eds C. M. Lambert and C. G. Granqvist), Institute Series, Opt. Eng. Press, Bellingham, USA, 1990, p. 471
7 Hrai, Y. and Tapi, C. *Appl. Phys. Lett.* 1983, **43,** 704
8 Przyluski, J. and Wieczorek, W. *Synth. Met.* 1991, **45,** 323
9 Gray, F. M. in 'Solid Polymer Electrolytes—Fundamentals and Technological', VCH, Weinheim, Germany, 1991, Ch. 6
10 Cheradame, H. and Le Nest, J. F. in 'Polymer Electrolyte Reviews 1' (Eds J. R. MacCallum and C. A. Vincent), Elsevier, London, 1987, p. 103
11 Gibson, P. E., Vallance, M. A. and Cooper, S. L. in 'Developments in Block Copolymers', Elsevier, Applied Science, London, 1982
12 Van Bogart, J. V., Gibson, P. E. and Cooper, S. L. *J. Polym. Sci., Polym. Phys. Edn* 1983, **21,** 65
13 Dickinson, L. C., Shi, J. and Chien, J. C. W. *Macromolecules* 1992, **25,** 1224
14 Kricheldorf, H. R. and Hull, W. E. *Makromol. Chem.* 1981, **182,** 1177
15 Leung, L. M. and Koberstein, J. T. *J. Polym. Sci., Polym. Phys. Edn* 1985, **23,** 1883
16 Miller, J. A. and Cooper, S. L. *J. Polym. Sci., Polym. Phys. Edn* 1985, **23,** 1065
17 Li, Y., Gao, T. and Chu, B. *Macromolecules* 1992, **25,** 1737
18 Seymour, R. W. and Cooper, S. L. *Macromolecules* 1973, **6,** 48
19 Hesketh, T. R., Van Bogart, J. W. C. and Cooper, S. L. *Polym. Eng. Sci.* 1980, **20,** 190
20 Koberstein, J. T. and Galambos, A. F. *Macromolecules* 1992, **25,** 5618
21 Leung, L. M. and Koberstein, J. T. *Macromolecules* 1986, **19,** 706
22 Srichatrapimuk, V. W. and Cooper, S. L. *Macromol. Sci.—Phys. B* 1978, **15,** 267
23 Senich, S. A. and MacKnight, W. J. *Macromolecules* 1980, **13,** 106
24 Lee, H. S., Wang, Y. K. and Hsu, S. L. *Macromolecules* 1987, **20,** 2089
25 Coleman, M. M., Lee, K. H., Skrovanek, D. J. and Painter, P. C. *Macromolecules* 1986, **19,** 2149
26 Coleman, M. M., Skrovanek, D. J., Howe, S. E. and Painter, P. C. *Macromolecules* 1985, **18,** 299
27 Sei, M. and Sato, K. *Makromol. Chem.* 1992, **193,** 2971
28 McLennaghan, A. W. and Pethrick, R. A. *Eur. Polym. J.* 1988, **24,** 1063
29 McLennaghan, A. W., Hooper, A. and Pethrick, R. A. *Eur. Polym. J.* 1989, **25,** 1297
30 Marcott, C., Noda, I. and Dowrey, A. E. *Anal. Chim. Acta* 1991, **250,** 131
31 Noda, I. *Appl. Spectrosc.* 1990, **44,** 550
32 Watanabe, M., Oohashi, S., Sanui, K., Ogata, N., Kobayashi, T. and Ohtaki, Z. *Macromolecules* 1985, **18,** 1945
33 Watanabe, M., Sanui, K. and Ogata, N. *Macromolecules* 1986, **19,** 815
34 Schantz, S., Torell, L. M. and Stevens, J. R. *J. Appl. Phys.* 1988, **64**(4), 2038
35 Stevens, J. R. and Schantz, S. *Polym. Commun.* 1988, **29,** 330
36 Chung, S. H., Such, K., Wieczorek, W. and Stevens, J. R. *J. Polym. Sci., Polym. Phys. Edn.* 1994, **32,** 2733
37 Kakihana, M., Schantz, S. and Torell, L. M. *J. Chem. Phys.* 1990, **92,** 6271
38 Schantz, S., Torell, L. M. and Stevens, J. R. *J. Chem. Phys.* 1991, **94,** 6862
39 Venkatasetty, H. V. *J. Electrochem. Soc.* 1975, **122,** 245
40 van Heumen, J. D. and Stevens, J. R. *Macromolecules* 1995, **28,** 4268
41 Schantz, S. *J. Chem. Phys.* 1991, **94,** 6296
42 Bernson, A. and Lindgren, J. *Polymer* 1994, **35,** 4848
43 James, D. W. and Mayes, R. E. *J. Chem. Phys.* 1984, **88,** 637
44 Berne, B. J. and Pecora, R. in 'Dynamic Light Scattering, with Applications to Chemistry, Biology, and Physics', John Wiley & Sons, New York, 1976, p. 370